

**RUST CONVERSION STUDIES OF
ARCHEOLOGICAL IRONS FROM FORT
CORNWALLIS USING MODIFIED OIL PALM
FRONDS LIGNIN**

LIYANA SYAFAWATI BINTI OSMAN

UNIVERSITI SAINS MALAYSIA

2024

**RUST CONVERSION STUDIES OF
ARCHEOLOGICAL IRONS FROM FORT
CORNWALLIS USING MODIFIED OIL PALM
FRONDS LIGNIN**

by

LIYANA SYAFAWATI BINTI OSMAN

**Thesis submitted in fulfillment of the requirements
for the degree of
Master of Science**

September 2024

ACKNOWLEDGEMENT

First and foremost, I want to express my gratitude to my main supervisor, Associate Professor Dr. Mohd Hazwan Hussin, and my co-supervisor, Professor Dr. Mohamad Nasir Mohamad Ibrahim from Universiti Sains Malaysia for their support, guidance, advice, and assistance throughout this research. I also would like to express my gratitude to Professor Nicolas Brosse, Associate Professor Dr. Isabelle Ziegler-Devin, and Dr. Laurent Chrusciel from Universite de Lorraine, Nancy, France for the endless guidance, support, and assistance throughout my 3 months of attachment in Nancy, France for this research.

I sincerely appreciate the Ministry of Higher Education through the Prototype Research Grant Scheme, PRGS (PRGS/1/2022/STG05/USM/02/1) and Postgraduate Research Attachment, PGRA from Institute Postgraduate Studies, Universiti Sains Malaysia for their financial support throughout this research. I also would like to thank Pusat Penyelidikan Arkeologi Global, USM for providing archeological samples for my research studies. And special thanks to all the administrative and technical staff, especially laboratory assistants and science officers at the School of Chemical Sciences, USM, and LERMAB, Faculte de Science and Technologies, UL for their assistance during my master's studies.

Besides, my sincere appreciation goes to all my friends and lecturers for dedicating their time to assist me in finishing my studies. Last but not least, a special thanks to both of my parents and my siblings for their unwavering support, understanding, and ongoing prayers during my master's studies and beyond.

TABLE OF CONTENTS

ACKNOWLEDGEMENT	ii
TABLE OF CONTENTS	iii
LIST OF TABLES	vii
LIST OF FIGURES	x
LIST OF SYMBOLS	xv
LIST OF ABBREVIATIONS	xvii
LIST OF APPENDICES	xix
ABSTRAK	xx
ABSTRACT	xxii
CHAPTER 1 INTRODUCTION	1
1.1 Background of the study	1
1.2 Problem statement	3
1.3 Research objectives	4
1.4 Scope of the study	5
CHAPTER 2 LITERATURE REVIEW	6
2.1 Archeological irons rust	6
2.1.1 Fort Cornwallis	10
2.2 Corrosion-controlling techniques	11
2.3 Overview of rust conversion studies	13
2.4 Lignocellulosic biomass	16
2.5 Oil palm (<i>Elaeis guineensis</i>)	20
2.6 Lignin	21

2.7	Delignification process	24
2.7.1	Organosolv pulping	24
2.8	Combinative pretreatment process	26
2.8.1	Autohydrolysis pretreatment.....	28
2.8.2	Steam explosion pretreatment	30
2.8.3	Incorporation of organic scavengers during pretreatment process	33
CHAPTER 3 EXPERIMENTAL		36
3.1	Materials and chemicals.....	36
3.2	Autohydrolysis pretreatment with organic scavengers	39
3.3	Steam explosion pretreatment.....	39
3.4	Extraction of lignin <i>via</i> organosolv pulping.....	41
3.5	Characterizations of extracted organosolv lignin	41
3.5.1	Elemental analysis.....	41
3.5.2	Fourier transform infrared (FTIR) analysis.....	42
3.5.3	Acetylation of lignin for nuclear magnetic resonance and gel permeation chromatography analyses	42
3.5.4	Nuclear magnetic resonance (NMR) spectroscopy.....	43
3.5.5	Gel permeation chromatography (GPC) analysis.....	43
3.5.6	Thermal analyses	43
3.5.7	Solubility test	44
3.5.8	Antioxidant activity by ferric reducing power assay.....	45
3.6	Archeological irons	46
3.6.1	Preparation of rust powder from archeological irons	46
3.6.2	Characterization of archeological irons rust powder.....	47

3.6.2(a)	Fourier transform infrared (FTIR) analysis.....	47
3.6.2(b)	Ionic chromatography (IC) analysis.....	47
3.6.2(c)	X-ray diffraction (XRD) analysis.....	47
3.6.2(d)	X-ray fluorescence (XRF) analysis.....	48
3.6.2(e)	Surface analysis.....	48
3.7	Rust conversion studies	48
3.7.1	Rust treatment with various organosolv lignin	48
3.7.1(a)	Effect of concentrations.....	48
3.7.1(b)	Effect of pH	49
3.7.1(c)	Effect of reaction time.....	50
3.7.2	Characterization of treated rusts	50
CHAPTER 4 RESULTS AND DISCUSSIONS.....		51
4.1	Proximate analysis	51
4.2	Characterization of extracted organosolv lignin	53
4.2.1	Elemental analysis	53
4.2.2	FTIR analysis.....	54
4.2.3	¹ H and ¹³ C NMR spectroscopy.....	58
4.2.4	2D-NMR HSQC and HMBC spectroscopy.....	62
4.2.5	GPC analysis.....	68
4.2.6	Thermal analyses.....	69
4.2.7	Solubility test	74
4.2.8	Antioxidant activity by ferric reducing power assay.....	75
4.3	Characterizations of archeological irons rust powder	77
4.3.1	FTIR analysis	77
4.3.2	Ionic chromatography (IC) analysis	78

4.3.3	X-ray diffraction (XRD) analysis.....	79
4.3.4	X-ray fluorescence (XRF) analysis.....	82
4.3.5	Surface analysis	84
4.3.5(a)	SEM-EDX analysis.....	84
4.4	Rust conversion studies.....	86
4.4.1	Rust treatment with various organosolv lignin	86
4.4.1(a)	Effect of concentrations	86
4.4.1(b)	Effect of pH	92
4.4.1(c)	Effect of reaction time	97
4.4.2	Characterizations of treated rusts	103
4.4.2(a)	XRD analysis	103
4.4.2(b)	SEM-EDX analysis.....	105
4.4.3	Mechanism of rust conversion studies	110
CHAPTER 5 CONCLUSION AND FUTURE RECOMMENDATIONS		112
5.1	Conclusion	112
5.2	Future recommendations.....	113
REFERENCES		115
APPENDICES		
LIST OF PUBLICATIONS		
LIST OF AWARDS		

LIST OF TABLES

	Page
Table 2.1	Hydrolysis products of iron cations at various pH values (Ribun et al., 2022)..... 7
Table 2.2	List of previous studies on rust conversion studies and their rate of transformation 15
Table 2.3	Different lignocellulosic biomass with its compositions..... 18
Table 4.1	Elemental composition of extracted organosolv lignin samples from OPF (%w/w on dry matter)..... 54
Table 4.2	FTIR assignment bands for organosolv lignin samples extracted from OPF 56
Table 4.3	Signals assignments of ¹³ C NMR spectroscopy for acetylated organosolv lignin samples 62
Table 4.4	GPC analysis of acetylated organosolv lignin samples (AH EOL, AHD EOL, AHPB EOL, and SEA EOL).....68
Table 4.5	Percentage atomic of elemental distribution on archeological irons' surfaces 83
Table 4.6	Atomic percentage of archeological irons (H.W.N and R.S) rust powder 85
Table 4.7	Rust transformation percentage values of archeological iron hand-wrought nail (H.W.N) rust powder treated with 1 wt.%, 3 wt.%, 5 wt.%, and 7 wt.% of AH EOL, AHD EOL, AHPB EOL, and SEA EOL 91

Table 4.8	Rust transformation percentage values of archeological iron railroad spike (R.S) rust powder treated with 1 wt.%, 3 wt.%, 5 wt.%, and 7 wt.% of AH EOL, AHD EOL, and AHPB EOL	91
Table 4.9	Rust transformation percentage values of archeological iron hand-wrought nail (H.W.N) rust powder treated with pH 1, pH 3, pH 5, pH 7, and pH 9 of 7 wt.% AH EOL, AHD EOL, AHPB EOL, and SEA EOL.....	96
Table 4.10	Rust transformation percentage values of archeological iron railroad spike (R.S) rust powder treated with pH 1, pH 3, pH 5, pH 7, and pH 9 of 7 wt.% AH EOL, AHD EOL, and AHPB EOL	97
Table 4.11	Rust transformation percentage values of archeological iron hand-wrought nail (H.W.N) rust powder treated at 1 day, 3 days, 5 days, 7 days, and 14 days of 7 wt.% AH EOL, AHD EOL, AHPB EOL, and SEA EOL	102
Table 4.12	Rust transformation percentage values of archeological iron railroad spike (R.S) rust powder treated at 1 day, 3 days, 5 days, 7 days, and 14 days of 7 wt.% AH EOL, AHD EOL, and AHPB EOL.....	103
Table 4.13	Atomic percentage of treated archeological iron hand-wrought nail (H.W.N) rust powder with various organosolv lignin samples	109

Table 4.14	Atomic percentage of treated archeological iron railroad spike (R.S) rust powder with various organosolv lignin samples	109
------------	---	-----

LIST OF FIGURES

	Page
Figure 2.1	Corrosion layer on archeological irons corroded in the atmosphere (Degrigny et al., 2007)..... 9
Figure 2.2	Excavation of cannons and mortars at Fort Cornwallis in 2019 (Ali, 2020)..... 11
Figure 2.3	Major components of lignocellulosic biomass (Banu et al., 2021) 17
Figure 2.4	Main phenylpropanoid units of lignin (Katahira et al., 2018; Mei et al., 2019; Nasrun et al., 2023)..... 22
Figure 2.5	Several linkages in the lignin structures (Katahira et al., 2018; Mei et al., 2019; Schutyser et al., 2018) 23
Figure 2.6	Possible mechanism during organosolv pulping process (Rabelo et al., 2023)..... 26
Figure 2.7	Various types of pretreatment processes on lignocellulosic biomass (Baruah et al., 2018; Latif et al., 2018; Tayyab et al., 2018)..... 27
Figure 2.8	Schematic illustration of the pretreatment process applied to lignocellulosic biomass (Muley & Boldor, 2017) 28
Figure 2.9	Possible mechanism during the autohydrolysis pretreatment process (Yan et al., 2016)..... 30
Figure 2.10	Schematic diagram of steam explosion pretreatment (Ma et al., 2022) 31

Figure 2.11	Possible mechanism of heterolytic pathway and homolytic pathway of β -O-4 linkages (Obame et al., 2019).....	34
Figure 3.1	Overview of procedural steps of this study.....	38
Figure 3.2	Schematic experiment of steam explosion pretreatment for OPF impregnated with 1% diluted sulfuric acid.....	40
Figure 3.3	(A) Fine powdered rust scraped from archeological iron hand-wrought nail and (B) fine powdered rust scraped from archeological iron railroad spike	46
Figure 4.1	Fingerprint region of FTIR spectra of AH EOL, AHD EOL, AHPB EOL, and SEA EOL	55
Figure 4.2	^1H NMR spectra of acetylated organosolv lignin (AH EOL, AHD EOL, AHPB EOL, and SEA EOL)	58
Figure 4.3	(A) Expanded aromatic region, (B) ^{13}C NMR spectra of acetylated organosolv lignin samples	60
Figure 4.4	2D-HSQC NMR spectroscopy of acetylated AH EOL, AHD EOL, AHPB EOL, and SEA EOL	65
Figure 4.5	Proposed interaction from 2D-HMBC NMR spectra of acetylated (a) AHD EOL, and (b) AHPB EOL	66
Figure 4.6	Proposed mechanism of lignin incorporated with 1,5-dihydroxy naphthalene	67
Figure 4.7	Proposed mechanism of lignin incorporated with <i>p</i> -benzoquinone	67
Figure 4.8	TG curves of organosolv lignin samples (AH EOL, AHD EOL, AHPB EOL, and SEA EOL)	71

Figure 4.9	DTG curves of organosolv lignin samples (AH EOL, AHD EOL, AHPB EOL, and SEA EOL)	72
Figure 4.10	DSC thermograms of organosolv lignin samples (AH EOL, AHD EOL, AHPB EOL, and SEA EOL),.....	73
Figure 4.11	Solubility of various organosolv lignin samples in water	75
Figure 4.12	Antioxidant activity of organosolv lignin samples <i>via</i> ferric reducing power assay at 700 nm	76
Figure 4.13	FTIR spectra of rust standards and archeological irons; (a) lepidocrocite (Lt), (b) goethite (Gt), (c) magnetite (Mt), (d) hand-wrought nail (H.W.N), and (e) railroad spike (R.S).....	78
Figure 4.14	IC chromatograms of rust powder from archeological irons (H.W.N and R.S).....	79
Figure 4.15	The XRD spectra of archeological irons rust powder: (A) hand-wrought nail (H.W.N) and (B) railroad spike (R.S).....	81
Figure 4.16	Micro-XRF spectra of archeological irons rust powder: (A) hand-wrought nail (H.W.N) and (B) railroad spike (R.S).....	83
Figure 4.17	SEM-EDX analysis for archeological irons rust powder: (A) hand-wrought nail (H.W.N) and (B) railroad spike (R.S).....	85
Figure 4.18	The FTIR spectra of treated archeological iron hand-wrought nail (H.W.N) rust powder at different concentrations (a) 1 wt.%, (b) 3 wt.%, (c) 5 wt.%, and (d) 7 wt.% of (A) AH EOL, (B) AHD EOL, (C) AHPB EOL, and (D) SEA EOL	88

Figure 4.19	The FTIR spectra of treated archeological iron railroad spike (R.S) rust powder at different concentrations (a) 1 wt.%, (b) 3 wt.%, (c) 5 wt.%, and (d) 7 wt.% of (A) AH EOL, (B) AHD EOL, and (C) AHPB EOL.....	89
Figure 4.20	The FTIR spectra of treated archeological iron hand-wrought nail (H.W.N) rust powder at different pH readings (a) pH 1, (b) pH 3, (c) pH 5, (d) pH 7, and (e) pH 9 of (A) AH EOL, (B) AHD EOL, (C) AHPB EOL, and (D) SEA EOL	94
Figure 4.21	The FTIR spectra of treated archeological iron railroad spike (R.S) rust powder at different pH readings (a) pH 1, (b) pH 3, (c) pH 5, (d) pH 7, and (e) pH 9 of (A) AH EOL, (B) AHD EOL, and (C) AHPB EOL	95
Figure 4.22	The FTIR spectra of treated archeological iron hand-wrought nail (H.W.N) rust powder at different reaction times (a) 1 day, (b) 3 days, (c) 5 days, (d) 7 days, and (e) 14 days of (A) AH EOL, (B) AHD EOL, (C) AHPB EOL, and (D) SEA EOL.....	100
Figure 4.23	The FTIR spectra of treated archeological iron railroad spike (R.S) rust powder at different reaction times (a) 1 day, (b) 3 days, (c) 5 days, (d) 7 days, and (e) 14 days of (A) AH EOL, (B) AHD EOL, and (C) AHPB EOL	101

Figure 4.24	XRD spectra of rust powder from archeological iron hand-wrought nail (H.W.N) (a) before treatment and after treatment with (b) 7 wt.% AH EOL, (c) 7 wt.% AHD EOL, (d) 7 wt.% AHPB EOL, and (e) 7 wt.% SEA EOL	104
Figure 4.25	XRD spectra of rust powder from archeological iron railroad spike (R.S) (a) before treatment and after treatment with (b) 7 wt.% AH EOL, (c) 7 wt.% AHD EOL, and (d) 7 wt.% AHPB EOL	105
Figure 4.26	SEM-EDX analysis of treated archeological iron hand-wrought nail (H.W.N) rust powder with (A) 7 wt.% AH EOL, (B) 7 wt.% AHD EOL, (C) 7 wt.% AHPB EOL, and (D) 7 wt.% SEA EOL	107
Figure 4.27	SEM-EDX analysis of treated archeological iron railroad spike (R.S) rust powder with (A) 7 wt.% AH EOL, (B) 7 wt.% AHD EOL, and (C) 7 wt.% AHPB EOL.....	108
Figure 4.28	Proposed mechanism of rust conversion studies using modified organosolv lignin incorporated with 1,5-dihydroxy naphthalene.....	111
Figure 4.29	Proposed mechanism of rust conversion studies using modified organosolv lignin incorporated with <i>p</i> -benzoquinone	111

LIST OF SYMBOLS

A	Absorbance of organosolv lignin samples
A_o	Absorbance of distilled water
Ar	Aromatic ring
C	Carbon
Cl^-	Chloride ions
C_L	Organosolv lignin concentration ($g L^{-1}$)
C_{max}	Maximum concentration of organosolv lignin samples
D	Dissolution
DTG_{max}	Maximum rate of weight loss
Fe	Iron
FL	Ferric lignin
G	Guaicyl (coniferyl alcohol unit)
Gt	Goethite (rust standard)
H	<i>p</i> -hydroxyphenyl (<i>p</i> -coumaryl alcohol unit)
K	Absorption constant ($2l L g^{-1} cm^{-1}$)
Lt	Lepidocrocite (rust standard)
M	Molarity
$m_{initial}$	Initial mass of organosolv lignin
M_n	Average molecular number
Mt	Magnetite (rust standard)
M_w	Average molecular weight
O	Oxygen
PDI	Polydispersity

PO_4^{3-}	Phosphate ions
ppm	Parts per million
rpm	Revolutions per minute
RT	Rate of transformation
S	Syringyl (sinapyl alcohol unit)
SF	Severity factor
S:L	Solid-to-liquid ratio
T	Reaction temperature ($^{\circ}\text{C}$)
T_g	Glass transition
t_s	Residence time (min)
TG	Thermal degradation weight loss
V_{total}	Total volume used
v/v	Volume per volume
wt.	Weight concentration
w/v	Weight per volume
w/w	Weight per weight
θ	Phase angle

LIST OF ABBREVIATIONS

AH EOL	Autohydrolysis organosolv lignin
AHD EOL	Autohydrolysis 1,5-dihydroxy naphthalene organosolv lignin
AHP EOL	Autohydrolysis <i>p</i> -nitrophenol organosolv lignin
AHPB EOL	Autohydrolysis <i>p</i> -benzoquinone organosolv lignin
CHNS/O	Carbon, hydrogen, nitrogen, and sulfur/oxygen analyzer
DBE	Double bond equivalent
DSC	Differential-scanning calorimeter
EDX	Energy-dispersive X-ray spectroscopy
FTIR	Fourier transform infrared
FRAP	Ferric reducing power assay
GPC	Gel permeation chromatography
HMBC	Heteronuclear multiple bonds correlation
HSQC	Heteronuclear single quantum correlation
H.W.N	Hand-wrought nail
IC	Ionic chromatography
KBr	Potassium bromide
NMR	Nuclear magnetic resonance
OPF	Oil palm fronds
R.S	Railroad spike
SEA EOL	Steam explosion acid impregnation organosolv lignin
SEM	Scanning electron microscope
TGA	Thermogravimetric analysis
THF	Tetrahydrofuran

UV-Vis	Ultraviolet-Visible spectrophotometer
XRD	X-ray diffraction
XRF	X-ray fluorescence

LIST OF APPENDICES

- Appendix A Full FTIR spectra of organosolv lignin samples
- Appendix B 2D-NMR HMBC spectra of modified organosolv lignin samples
- Appendix C DSC thermograms of organosolv lignin samples
- Appendix D Calculation of chloride ion (Cl^-) from IC
- Appendix E Calculation of phosphate ion (PO_4^{3-}) from IC
- Appendix F Rate of transformation (RT%) calculation
- Appendix G XRD spectra of treated archeological hand-wrought nail
- Appendix H XRD spectra of treated archeological railroad spike

**KAJIAN PENUKARAN KARAT BESI ARKEOLOGIKAL DARIPADA FORT
CORNWALLIS MENGGUNAKAN LIGNIN PELEPAH KELAPA SAWIT
TERMODIFIKASI**

ABSTRAK

Penyelidikan ini mendedahkan struktur dan sifat antioksidan bagi sampel lignin organosolv yang telah diekstrak daripada pelepah kelapa sawit (OPF) dengan kaedah pra-rawatan autohidrolisis apabila digabungkan dengan 1,5-dihidroksi naffalena (AHD EOL) dan *p*-benzokuinon (AHPB EOL) dan pra-rawatan letupan wap yang diimpregnasikan dengan asid sulfurik cair (SEA EOL). Didapati bahawa AHPB EOL mempunyai hasil peratusan tertinggi berbanding lignin organosolv yang lain (% yield AHPB EOL: $13.79 \pm 0.17\%$ > % yield SEA EOL: $13.66 \pm 0.35\%$ > % yield AHD EOL: $13.09 \pm 1.03\%$ > % yield AH EOL: $12.40 \pm 1.18\%$). Kemudian, pelbagai lignin organosolv telah dianalisa menggunakan analisis pelengkap seperti analisis unsur, Inframerah Transformasi Fourier (FTIR), spektroskopi resonans nuclear magnetik (NMR), kromatografi gel penyerapan (GPC), analisis termogravimetrik (TGA), kalorimetri pengimbas berbeza (DSC), ujian keterlarutan, dan aktiviti antioksidan. Sepanjang analisa dijalankan, lignin organosolv termodifikasi (AHD EOL dan AHPB EOL) dan lignin organosolv asid pra-rawatan letupan wap (SEA EOL) mempamerkan matriks lignin lebih kecil dengan kandungan fenolik yang lebih tinggi (fenolik-OH SEA EOL: 0.60/Ar > fenolik-OH AHPB EOL: 0.47/Ar > fenolik-OH AHD EOL: 0.45/Ar > fenolik-OH AH EOL: 0.40/Ar), yang membawa kepada keterlarutan air (D% SEA EOL: $29.50 \pm 0.11\%$ > D% AHPB EOL: $24.25 \pm 0.13\%$ > D% AHD EOL: $22.50 \pm 0.16\%$ > D% AH EOL: $20.50 \pm 0.22\%$) dan aktiviti antioksidan lebih tinggi berbanding sampel lignin organosolv yang tidak termodifikasi (AH EOL). Sampel lignin organosolv yang diekstrak kemudiannya digunakan dalam kajian penukaran

karat besi arkeologikal (paku tempa tangan dan penyucuk rel kereta api) dan menunjukkan bahawa paku tempa tangan arkeologikal yang dirawat mempunyai RT% optimum pada 7 wt.% SEA EOL dengan $95.45 \pm 0.13\%$ manakala bagi sampel penyucuk rel kereta api arkeologikal yang dirawat menunjukkan bahawa AHPB EOL pada kepekatan 7 wt.% mempunyai RT% tertinggi dengan $88.81 \pm 0.14\%$. Analisis XRD dan permukaan sampel karat arkeologikal yang dirawat juga menunjukkan bahawa ia telah berubah menjadi fasa amorfus.

RUST CONVERSION STUDIES OF ARCHEOLOGICAL IRONS FROM FORT CORNWALLIS USING MODIFIED OIL PALM FRONDS LIGNIN

ABSTRACT

This research reveals the structural and antioxidant properties of extracted organosolv lignin samples derived from oil palm fronds (OPF) pretreated with autohydrolysis upon incorporation with 1,5-dihydroxy naphthalene (AHD EOL) and *p*-benzoquinone (AHPB EOL) and steam explosion pretreatment impregnated with diluted sulfuric acid (SEA EOL). It was revealed that AHPB EOL had the highest percentage of yield among other organosolv lignin samples (% yield AHPB EOL: $13.79 \pm 0.17\%$ > % yield SEA EOL: $13.66 \pm 0.35\%$ > % yield AHD EOL: $13.09 \pm 1.03\%$ > % yield AH EOL: $12.40 \pm 1.18\%$). Various organosolv lignin samples were then evaluated with elemental analysis, Fourier transform infrared (FTIR), nuclear magnetic resonance (NMR), gel permeation chromatography (GPC), thermogravimetric (TGA), differential-scanning calorimeter (DSC), solubility test, and antioxidant activity. Throughout the analyses, modified organosolv lignin (AHD EOL and AHPB EOL) and steam explosion acid impregnation organosolv lignin (SEA EOL) exhibited smaller lignin matrix with higher phenolic content (phenolic-OH SEA EOL: 0.60/Ar > phenolic-OH AHPB EOL: 0.47/Ar > phenolic-OH AHD EOL: 0.45/Ar > phenolic-OH AH EOL: 0.40/Ar), which leads to higher water solubility (D% SEA EOL: $29.50 \pm 0.11\%$ > D% AHPB EOL: $24.25 \pm 0.13\%$ > D% AHD EOL: $22.50 \pm 0.16\%$ > D% AH EOL: $20.50 \pm 0.22\%$) and antioxidant activity compared to unmodified organosolv lignin (AH EOL). The extracted organosolv lignin samples were then utilized in rust conversion studies of archeological irons (hand-wrought nail and railroad spike) and indicated that the treated archeological hand-wrought nail possessed the optimum RT% at 7 wt.% SEA EOL with $95.45 \pm 0.13\%$ whereas for

treated archeological railroad spike indicated AHPB EOL at a concentration of 7 wt.% possessed the highest RT% with $88.81 \pm 0.14\%$. The XRD and surface analysis of the treated archeological rust also showed that it had transformed into amorphous phases.

CHAPTER 1

INTRODUCTION

1.1 Background of the study

Metallic items can still corrode even after being relocated. This is due to the deteriorating process when exposed to a corrosive environment (Abdel-Karim & El-Shamy, 2022). Chemical interactions between metals and their surrounding environment can lead to degradation (Abdrabo et al., 2020). Rust products are characterized as a complex process of continual transformation resulting from precipitation, evolution, and transformation of chemical species within the iron-oxygen-water system (Dahon et al., 2018). Preserving archeological iron artifacts is a worthwhile investment because of their historical significance and importance to economic sectors, particularly in attracting tourists. Therefore, various treatments have been employed to inhibit further corrosion on the archeological irons (Salem et al., 2019).

One of the promising methods to inhibit further corrosion on the archeological irons is rust conversion study. The rust conversion study utilizes rust converter agents which are chemicals that can convert rust into a durable and attached black film of chemical compounds on corroded iron (Zhao et al., 2014). In this method, rust converter agents are applied to rusty surfaces to convert rust into a harmless protective layer that allows for overcoating (Saji, 2019). This barrier will slow down the metal's redox reactions and decrease the breakdown of the defense system. The anticipated value of the worldwide anti-corrosion coatings market is expected to reach US\$ 38.6 billion by 2027 (Grand View Research, 2020).

Over the past decades, the worldwide consumption of energy has expanded tremendously. According to recent studies by Trache et al. (2020) and Tsegaye et al. (2019), the significant increase in the scarcity of petroleum/fossil-based economy is accelerating the rate of climate change. Consequently, the research community has demonstrated substantial interest in exploiting biomass waste as an alternate strategy to transition from a petroleum/fossil-based economy to a bio-based economy. Lignocellulosic biomass, such as oil palm is widely planted in Malaysia for its substantial usage in their varied portions (Parveez et al., 2023). A significant amount of agro-industrial waste, such as oil palm fronds (OPF), is generated roughly 70% during replanting activities per year (Lee et al., 2021). Studies claimed that OPF is usually used to develop bio-based economic items due to its diverse usefulness and advantageous utilization in power generation, electricity production, biodiesel production, and value-added chemicals production (Junior et al., 2016; Sa'don et al., 2017a).

Nowadays, the isolation of three primary components of lignocellulosic structures such as lignin, cellulose, and hemicellulose are extensively researched (Leng et al., 2022; Margellou et al., 2021). Among these significant components, lignin has garnered significant interest owing to its unique attributes and advantageous applications. Lignin is a complex and non-toxic natural resource with a varied range of functional groups in its structure, making it very promising for many industrial uses (Kane et al., 2021; Leng et al., 2022). Other than that, lignin is a valuable source of antioxidants due to its phenolic components and potent free radical scavenging properties (Barapatre et al., 2016; de Melo et al., 2020).

1.2 Problem statement

The National Association of Corrosion Engineers estimates that the worldwide cost of corrosion is US\$ 2.5 trillion/year, corresponding to 3.4% of global GDP (Koch et al., 2016). Archeological iron artifacts are often discovered to be more corroded and deteriorated compared to other artifacts due to their exposure to metal activities. Archeological irons retrieved from underground, or water are prone to experiencing physical, chemical, or biological transformations due to interactions with their burial environment. Previous studies have shown that preserving archeological irons can be challenging, particularly in a high-humidity environment. The archeological irons exhibit increased brittleness and are prone to rapid rusting (Armetta et al., 2021; Bernabale et al., 2022; Jia et al., 2022).

Recently, various treatments were used to inhibit further corrosion from occurring on the metal artifacts. One of the rapid methods for treating archeological irons is rust conversion study. However, the currently accessible rust converter agents utilized in rust conversion studies are primarily based on tannic acid and phosphoric acid, which exhibit significant toxicity, prompting researchers to explore alternatives that are safer and more environmentally sustainable (Merino et al., 2017). Prior studies mentioned that the metal surface will be further corroded if there is excessive acid presence post-treatment (Wei et al., 2020; P. Yu et al., 2022). Therefore, rust converter agents derived from natural plant-based products are being considered as they contain active substances to halt additional corrosion on the archeological irons (Jia et al., 2022; Rozuli et al., 2019; Zouarhi, 2023).

In 2023, oil palm plantations in Malaysia reached 5.6 million hectares and will increase throughout the years (MPOB, 2023a). Thus, expanding oil palm plantations will lead to a rise in oil palm waste production. Inexplicably, these oil palm

wastes, particularly OPF, were intentionally left to decompose for mulching and recycling. Even so, this process is time-consuming and could lead to a massive environmental catastrophe (Latif et al., 2019; Sa'don et al., 2017b). Lignin derived from OPF has been utilized as anti-corrosion coatings by multiple researchers (Dastpak et al., 2018; Shah et al., 2017). However, the intricate lignin structure's resistance to water and low solubility have limited its promise for various industrial applications. Hence, it is essential to modify the lignin structure to achieve desired properties and overcome these constraints. Prior research showed that modified lignin structure resulted in smaller fragments with increased phenolic content, leading to improved solubility and enhanced antioxidant capabilities (Hussin et al., 2016; Latif et al., 2019). Improving the quality of the lignin structure will enhance its usefulness in various industrial applications, such as in rust conversion studies.

1.3 Research objectives

In this research study, the OPF biomass underwent different pretreatment processes which were autohydrolysis and steam explosion pretreatment. Organic scavengers such as 1,5-dihydroxy naphthalene and *p*-benzoquinone were utilized during autohydrolysis pretreatment, while diluted sulfuric acid was utilized for impregnation in the steam explosion pretreatment. This was followed by organosolv pulping to extract various organosolv lignin samples with smaller fragments and low molecular weight. The objectives of this research were as follows:

- 1) To modify the lignin structure extracted from OPF biomass with the addition of organic scavengers (1,5-dihydroxy naphthalene and *p*-benzoquinone) during autohydrolysis pretreatment and with the impregnation of diluted sulfuric acid during steam explosion pretreatment.

- 2) To characterize various extracted organosolv lignin samples using complementary analyses such as FTIR, NMR, GPC, TGA, DSC, solubility test, and antioxidant activity and archeological irons' rust powder (hand-wrought nail, H.W.N, and railroad spike, R.S) *via* FTIR, IC, XRD, XRF, and SEM-EDX.
- 3) To study the rate of transformation of archeological irons' rust with additional extracted organosolv lignin samples from OPF *via* varying concentrations, varying pH of the mixture, and varying reaction time.

1.4 Scope of the study

This research study involves employing lignin derived from OPF for rust conversion studies on archeological irons. The OPF biomass underwent pretreatment utilizing autohydrolysis with several organic scavengers such as 1,5-dihydroxy naphthalene and *p*-benzoquinone and steam explosion pretreatment impregnated with diluted sulfuric acid. Then, the pretreated OPF biomass was subjected to organosolv pulping. This study involves analyzing unmodified and modified organosolv lignin samples prior to their use in rust conversion studies on archeological irons. Other than that, this research also examines the effectiveness of unmodified and modified organosolv lignin samples on rust conversion studies of archeological irons at varying concentrations. Additionally, this research also aims to optimize rust conversion studies by altering the pH of the mixture and reaction times of the archeological irons treated with the most optimum concentrations of the rate of transformation (RT%) of different organosolv lignin samples. Subsequently, the surface properties of the treated rust were examined using a variety of complementary analyses.

CHAPTER 2

LITERATURE REVIEW

2.1 Archeological irons rust

Corrosion is the process of metals and alloys deterioration due to environmental oxidation. Zouarhi (2023) identified corrosion as a significant problem in the industrial sector resulting in the annual loss of 100 million tons of metals, equivalent to 15% of the world's production. It is crucial to address this issue as it may end up in severe destruction of archeological irons, leading to the loss of valuable information and details about the artifacts (Dwivedi & Mata, 2019). Archeological irons are susceptible to soil corrosion in different environments, which can lead to the deterioration of metal artifacts. Soil corrosion is an electrochemical process caused by dissolved salts in groundwater, which turn the soil into an electrolyte solution. The salinity levels can range from freshwater (> 0.1%) to brine solutions (5 – 40%). Soil pH levels fluctuate based on the overall mineral content of groundwater and the existence of acids, acidic compounds, and basic salts (Ribun et al., 2022).

During the burial of the archeological irons, the dissolution of iron takes place on the anodic site of the electrochemical process on the artifacts surfaces (Zouarhi, 2023):



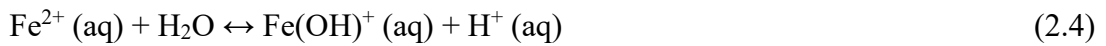
At the cathodic site of the electrochemical process with a pH of more than 4, the oxygen gas reactions take place, following scheme 2.2 (Ribun et al., 2022):



whereas at a lower pH than 4, hydrogen gas is produced at the cathodic site of the electrochemical process (Buravlev & Balagurova, 2021):



As the archeological irons corroded, the anodic and cathodic reactions become localized causing a decrease of potential differences in the anodic and cathodic polarization. Therefore, this will then reduce the corrosion current and its corrosion rate. The acidity in the anodic site increases due to the iron hydrolysis, impacting the formation of $\text{Fe}(\text{OH})^+$ and H^+ ions in the solution (Buravlev & Balagurova, 2021):



According to a prior study by Ribun et al. (2022), a small amount of oxygen oxidized Fe^{2+} to Fe^{3+} . Fe^{3+} ions are then hydrated forming aqua complex $(\text{Fe}(\text{H}_2\text{O})_6)^{3+}$ which can also be hydrolyzed. The pH influenced the formation of different iron (II) and iron (III) species as shown in Table 2.1.

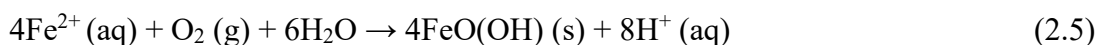
Table 2.1: Hydrolysis products of iron cations at various pH values (Ribun et al., 2022).

$(\text{Fe}(\text{H}_2\text{O})_6)^{2+}$ hydrolysis products		$(\text{Fe}(\text{H}_2\text{O})_6)^{3+}$ hydrolysis products	
Fe^{2+}	pH values	Fe^{3+}	pH values
$(\text{Fe}(\text{H}_2\text{O})_6)^{2+}$	< 9	$(\text{Fe}(\text{H}_2\text{O})_6)^{3+}$	< 2
$\text{Fe}(\text{OH})^+$	9 – 10	$\text{Fe}(\text{OH})^{2+}$	2 – 3.5
$\text{Fe}(\text{OH})_3^-$	> 10	$\text{Fe}(\text{OH})_2^+$	3.5 – 8.5
$\text{Fe}(\text{OH})_4^{2-}$	> 10	$\text{Fe}(\text{OH})_4^-$	> 8.5

Iron (III) hydroxide becomes insoluble when the pH is more than 6. Once emerged, it is oxidized to produce compounds such as magnetite (Fe_3O_4) and iron (III) compounds such as hydroxide and oxyhydroxide. Initially, $\text{Fe}(\text{OH})_3$ has an amorphous structure which gradually changes into crystalline oxyhydroxides like lepidocrocite

(γ -FeOOH), and eventually into a more stable compound such as goethite (α -FeOOH). Akaganéite (β -FeOOH) and chlorine derivatives like $\text{Fe}_2(\text{OH})_3\text{Cl}$ are formed due to the existence of Cl^- ions.

During the burial of the archeological irons, oxygen access is restricted, the temperature remains stable, the humidity is consistent, and there is no exposure to light. However, the excavation of the archeological irons speeds up their deterioration. The excavated metal artifacts are influenced by factors such as increased oxygen levels, excessive humidity, and fluctuating temperatures, which directly affect the quality of moisture films that develop on the metal artifact's surfaces (Buravlev & Balagurova, 2021). The newly wet excavated metal artifacts are filled with soil solution that contains Fe^{2+} , $\text{Fe}(\text{OH})^+$, H^+ , and Cl^- . As the metal artifacts dried, the chlorides contained in the pores of the metal artifacts put pressure on the pore walls of the metal artifacts, which led to cracking and destruction. The excess amount of oxygen oxidizes Fe^{2+} ions and forms an iron oxyhydroxide (Ribun et al., 2022):



Corrosion damages the physical shape of metal artifacts and chemically affects any remaining iron. The formation of new solids inside surface layers leads to physical damage by inducing stress and cracks, illustrated in Figure 2.1 (Degrigny et al., 2007). Iron oxyhydroxides forming on the archeological irons exert stress, resulting in cracking and destruction. This enhances oxygen availability and accelerates the corrosion process.

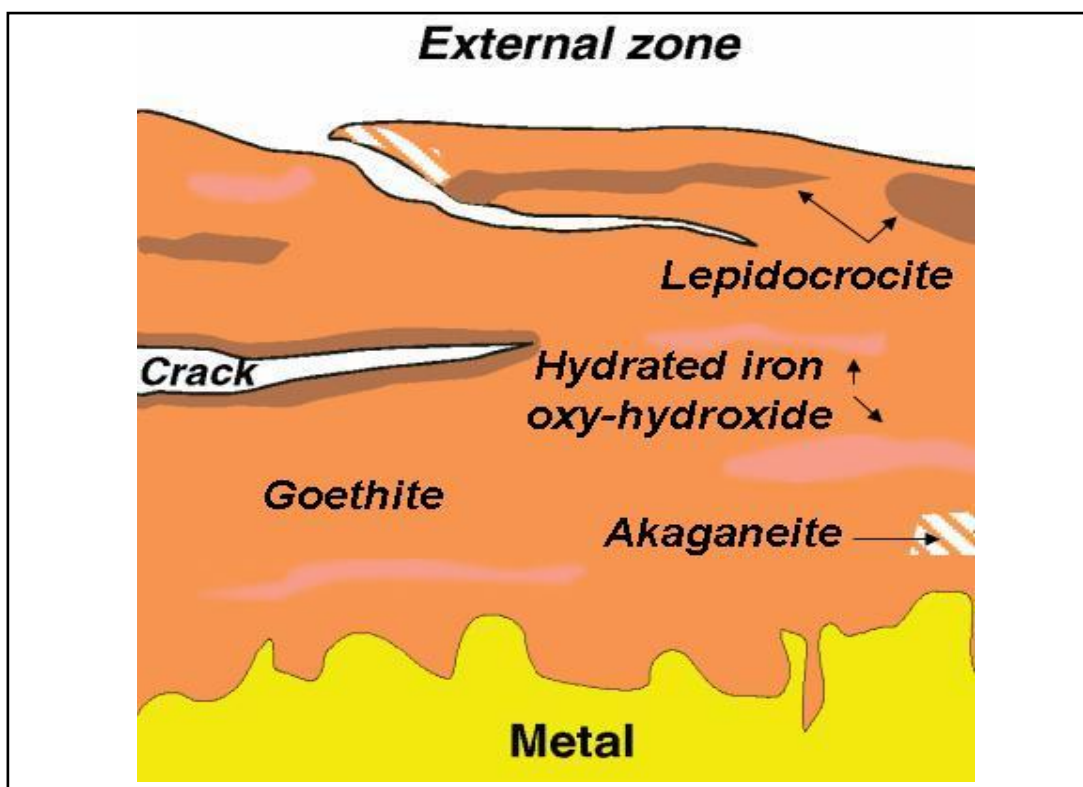


Figure 2.1: Corrosion layer on archeological irons corroded in the atmosphere (Degriigny et al., 2007).

Previous research indicated that iron (II) chloride exists as a yellow crystal ($\text{FeCl}_2 \cdot 2\text{H}_2\text{O}$) at a relative humidity below 20% and a green crystal ($\text{FeCl}_2 \cdot 4\text{H}_2\text{O}$) between 20 – 55% humidity. Under high humidity conditions, these salts absorb water, dissolve, and create orange liquid droplets where iron oxyhydroxides are formed, resulting in spherical shapes (Buravlev & Balagurova, 2021; Ribun et al., 2022). To summarize, the burial of the archeological irons involves corrosion such as Fe_3O_4 and FeOOH , which subsequently oxidize to $\alpha\text{-FeOOH}$ and $\gamma\text{-FeOOH}$. Following the excavation of the archeological irons, FeOOH , $\alpha\text{-FeOOH}$, $\gamma\text{-FeOOH}$, $\beta\text{-FeOOH}$, and Fe_3O_4 are present on the surfaces of the artifacts. A realistic method is required to regulate iron corrosion by either decreasing the corrosion rate or enhancing corrosion resistance.

2.1.1 Fort Cornwallis

Fort Cornwallis was established on Penang Island in 1786 by Captain Sir Francis Light. Their region, originally devoid of permanent structures, spanned 417.6 ft² and served as the first military and administrative outpost of the East India Company (EIC) in Southeast Asia. Fort Cornwallis was reconstructed in 1804 and filled with various buildings and features like military barracks and offices as well as a gunpowder magazine, a church, a harbor light, flagstaff, cannons, cell rooms, a store, and guard houses. Despite being constructed for military purposes, the fort's historical role was mostly administrative rather than defensive. The fort has never engaged in any battles during its history (Ju, 2023). Fort Cornwallis now spans 332859 ft², showcasing its ancient and rugged features. The fort has experienced structural deterioration, with just the gunpowder magazine, a church, cell rooms, flagstaff, harbor light, and several cannons still intact (Harun et al., 2002).

In 2018, Fort Cornwallis was allocated RM 5.8 million for the first phase of restoring the fort's storerooms from the state government and Think City Sdn Bhd (Lo, 2022). The budgets allotted approximately RM 7.2 million for the excavation and restoration of the moat in the south and west parts of the fort during phases two and phase three. The task was anticipated to be completed by late 2024 or early 2025 (Ong, 2022). During the excavations in 2018 and 2019, an estimated 30000 artifacts dating back to British rule and Japanese occupation were discovered. These relics included cannons, mortars, bottles, broken pieces of ceramics, and oil coins. Figure 2.2 depicted one of the cannons and mortars excavated from Fort Cornwallis in 2019.



Figure 2.2: Excavation of cannons and mortars at Fort Cornwallis in 2019 (Ali, 2020).

2.2 Corrosion-controlling techniques

Corrosion is a complex process that involves at least two phases, such as solid and liquid, solid and gas, or liquid and gas, and naturally happens in the aqueous phase (Komary et al., 2023). However, metal corrosion cannot be prevented but can be slowed down through monitoring or regulating the mechanism. Studies showed that corrosion on metal surfaces is more likely to happen in acidic solutions commonly utilized in industrial sectors involving acid cleaning, acid descaling, acid pickling, and oil well acidizing (Abdel-Karim & El-Shamy, 2022). Therefore, scientists are eager to create novel compounds that are non-toxic and more efficient to reduce corrosion. Several methods for controlling the rate of corrosion on metal surfaces include (i) material selection, (ii) material design, (iii) cathodic protection, (iv) coatings, (v) corrosion inhibitor, and (vi) rust conversion studies.

Corrosion on metal surfaces can manifest in several patterns and shapes, impacting the entire surface or specific sections. Thus, corrosion-resistant materials such as stainless steel and nickel alloy are frequently utilized in the oil and gas industry to inhibit further corrosion. Also, a well-designed tool can help prevent corrosion by eliminating heterogeneity. Varying metals, uneven tension, and temperature distribution are factors that can accelerate corrosion due to heterogeneity (Xie et al., 2023).

Other than that, corrosion can be prevented, controlled, or minimized using cathodic protection (Angst, 2019; Krishnan et al., 2021). This method pertains to metal submerged in an electrolytic solution, like seawater. Two primary strategies for cathodic protection systems commonly utilized in corrosion control are impressed current and sacrificial anode. Impressed current protection relies on an external electrical source to provide the protection current, while sacrificial anode utilizes active metal corrosion to supply the protection current owing to its higher negative potential (Cheng et al., 2022). Coatings, such as active metals, paints, oils, waxes, or powders applied to the metal surfaces and heated to create a thin protective layer that shields the metal from the atmosphere. A coated metal surface eliminates direct contact with a corrosive environment, therefore reducing the risk of corrosion (Ameh et al., 2017).

Corrosion inhibitors and rust conversion studies are acknowledged as cost-effective and dependable methods for managing corrosion on metal surfaces (Obot et al., 2019). These controlling techniques require only a minimal amount to be applied on the metal surfaces (Zakeri et al., 2022). These benefits have scientists keen to choose corrosion inhibitor and rust conversion studies from other corrosion-controlling techniques.

2.3 Overview of rust conversion studies

Rust conversion studies involve the use of rust converter agents to minimize and inhibit further corrosion (Dahon et al., 2018). The rust converter agents may convert rust on iron surfaces into a protective transformation film. This film acts as a barrier to prevent corrosive substances from reaching the metal surfaces (Abdulmajid et al., 2019). These rust converter agents work by reacting with iron oxides on the metal surfaces *via* redox reactions to prevent the breakdown of the protective system (Pereyra et al., 2006). Factors influencing the rust conversion on metal surfaces are the concentrations of rust converters, their pH levels, the reaction time between the rust converters and the rust on the metal surfaces, the presence of other materials, and the contamination levels of the rusted metals (Ocampo et al., 2004). Other than that, Rahim et al. (2011) indicated the rust transformation was also influenced by the temperature and the presence of air pollutants.

Formerly, rust converters composed of phosphoric acid and tannic acid were employed, however, their toxicity and lack of environmental friendliness caused harm to iron metal structures. This pertains to studies conducted by Collazo et al. (2008) and P. Yu et al. (2022), which found that if acid remains after treatment can infiltrate the inner substrate, leading to further corrosion on the internal metal surfaces. Therefore, naturally occurring polyphenols found in plants were selected as new green rust conversion agents. Plant-based rust converters are eco-friendly goods that contain multiple functional groups such as hydroxyl, carboxyl, amino groups, alkenes, and π -electrons centers, which provide a protective layer from inhibiting further corrosion (Ghuzali et al., 2021; Zakaria et al., 2022).

Various plant-based natural products utilized such as mangrove tannins (Rahim et al., 2011), tara tannins (Merino et al., 2017), gambir (Dahon et al., 2018), tamarind shell (Abdulmajid et al., 2019), Camphor tree (Yakubu et al., 2019), catechin (Jia et al., 2022), and coconut husk (Nasrun et al., 2023) have shown positive effects on rust conversion studies conducted by different researchers. Recent studies regarding the conversion of archeological rust showed that the archeological rust reacted positively with plant-based natural products such as catechin and lignin isolated from coconut husk (Jia et al., 2022; Nasrun et al., 2023). Nasrun et al. (2023) utilized soda and organosolv lignin extracted from coconut husk to treat archeological irons and obtained more than 80% of its rate of transformation at 5 wt.% of soda lignin. According to Jia et al. (2022) and Nasrun et al. (2023), the treated archeological rust changed to amorphous forms after it was treated with catechin and lignin, respectively.

Other than that, conversion studies tested on mild steel indicated that lepidocrocite occurred the fastest conversion compared to goethite and magnetite (Dahon et al., 2018; Rahim et al., 2011; Yakubu et al., 2019). Abdulmajid et al. (2019) extracted two distinct tamarind shell extracts and discovered that methanol extract (TME) yielded superior rust transformation outcomes compared to acetone extract (TAE). Table 2.2 indicates the list of previous rust conversion studies.

Table 2.2: List of previous studies on rust conversion studies and their rate of transformation.

References	Rust conversion ingredients	Remarks
Ocampo et al. (2004)	Phosphoric and tannic acid	No significant difference between treated and untreated rust
Rahim et al. (2011)	Mangrove tannins	Lepidocrocite converted into ferric tannins Rate of transformation : Lepidocrocite > Magnetite > Maghemite > Goethite
Merino et al. (2017)	Tara tannins	Lepidocrocite converted into ferric tannins
Dahon et al. (2018)	Gambir	10 wt.% of gambir concentration provided the optimum rate of transformation, 80% Rate of transformation: Lepidocrocite > Magnetite > Goethite
Abdulmajid et al. (2019)	Tamarind shell tannins	7 wt.% of TME possessed the best rate of transformation, 95.8% Rate of transformation: Lepidocrocite > Magnetite > Goethite
Yakubu et al. (2019)	Camphor tree	6 wt.% of methanol extract with a pH 4 solution had the most optimum rate of transformation, 96%
Jia et al. (2022)	Catechin	3.0 g/L catechin achieved a rust conversion efficiency of 73.26%
Nasrun et al. (2023)	Coconut husk	5 wt.% of soda lignin possessed the highest rate of transformation, 84.21%

2.4 Lignocellulosic biomass

Global energy demand has experienced substantial growth and is projected to rise by 28% by 2040 (Kumar et al., 2020). This will cause a major deterioration of the scarcity of petroleum/fossil-based economy, accelerating the rate of climate change such as global warming, acid rains, and glacial melting (Mankar et al., 2021). Therefore, the scientific community has displayed much enthusiasm for employing biomass waste as an alternative approach to transition from a petroleum/fossil-based economy to a bio-based economy. The objective is to attain the long-term goals of a sustainable circular economy that prominently focuses on using bio-based raw materials instead of the conventional industrial approach (Hassan et al., 2018).

Lignocellulosic biomass is recognized as a potential and promising resource of renewable energy due to its abundant raw material that reaches 200 billion tons/year (Ahmad et al., 2020). A study by Dahmen et al. (2019) stated that only 8.2 billion tons of lignocellulosic biomass were utilized. Approximately 7 billion tons were obtained from agricultural, grass, and forest land while the remaining 1.2 billion tons came from agricultural residues. However, only 3% of these biomass sources were utilized and integrated into the circular economy. Lignocellulosic biomass such as rice straw (Guan et al., 2018; Gundupalli et al., 2021), sugarcane (Bilatto et al., 2020; Gundupalli et al., 2021), corn stover (Khan et al., 2021; Wang et al., 2022), banana leaves (Shankar et al., 2020; Singh et al., 2020), wheat straw (Jin et al., 2022), oil palm (Latif et al., 2019; Sa'don et al., 2017a), coconut palm (Aziz et al., 2019; Nasrun et al., 2023), kenaf core (Hussin et al., 2019; Saratale et al., 2019), *Miscanthus Eucalyptus* (Babicka et al., 2022; Jung et al., 2015), bamboo (Chen et al., 2017; Ma et al., 2020), and pine wood (Darmawan et al., 2016; Magalhães et al., 2021) has been utilized for various future applications used such as biofuels, chemical, energy, and value-added products. This

is due to its abundant availability, cost-effectiveness, and environmentally sustainable nature (Kassaye et al., 2017).

Lignocellulosic biomasses are composed of three primary constituents such as cellulose (35 – 55%), hemicellulose (20 – 40%), and lignin (10 – 25%) with small amounts of extractives, protein, lipids, and ash as shown in Figure 2.3 (Banu et al., 2021). It can be found in hardwood, softwood, agricultural wastes, and grasses (Hassan et al., 2018). Different biomasses show different compositions of these major compounds as shown in Table 2.3. Nevertheless, the proportions of cellulose, hemicellulose, and lignin within a single plant are subject to variation due to factors such as age, harvesting season, and culture conditions (Hassan et al., 2018).

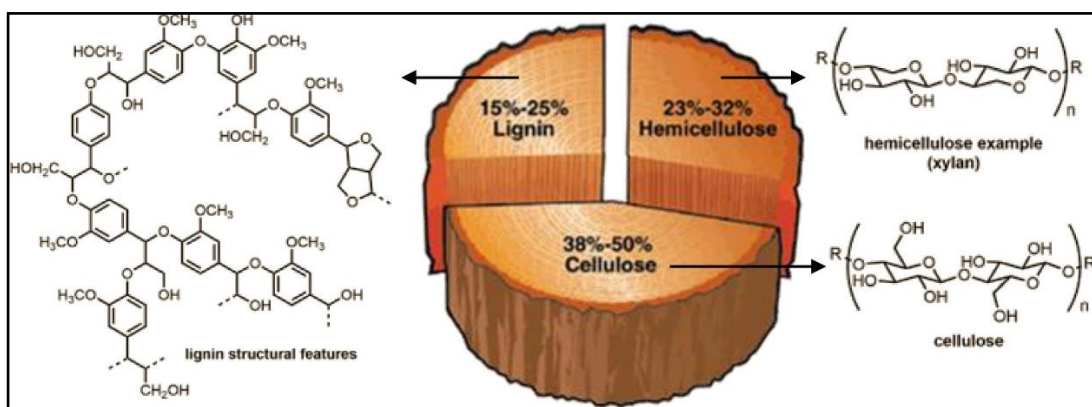


Figure 2.3: Major components of lignocellulosic biomass (Banu et al., 2021).

Table 2.3: Different lignocellulosic biomass with its compositions.

Lignocellulosic biomass	Cellulose (%)	Hemicellulose (%)	Lignin (%)	References
Rice straw	47.06 ± 1.68	25.35 ± 1.91	6.00 ± 1.10	(Gundupalli et al., 2021)
Sugarcane	29.70	35.60	28.40	(Bilatto et al., 2020)
Corn stover	35.16 ± 0.10	19.01 ± 0.05	18.82 ± 0.58	(Li et al., 2019)
Banana leaves	43.34	34.34	15.00	(Singh et al., 2020)
Wheat straw	34.72 ± 1.30	30.60 ± 2.27	10.39 ± 1.00	(Jin et al., 2022)
Oil palm fronds	21.83 ± 2.93	39.56 ± 2.77	20.08 ± 2.59	(Latif et al., 2019)
Oil palm mesocarp fiber	23.50	20.80	35.90	(Marques et al., 2020)
Coconut husks	27.19 ± 0.10	14.64 ± 0.70	37.93 ± 0.91	(Latif et al., 2022)
Kenaf core	28.85 ± 6.08	22.70 ± 3.37	22.22 ± 3.85	(Hussin et al., 2019)
<i>Miscanthus</i>	44.80 ± 0.20	25.20	20.00 ± 0.20	(Babicka et al., 2022)
<i>Eucalyptus</i>				
Bamboo	41.80	18.00	29.30	(Ma et al., 2020)
Pine wood	43.74	16.20	29.14	(Darmawan et al., 2016)

Cellulose is a polysaccharide composed of long chains of β -(1 – 4)-linked D-anhydroglucopyranose repeating units and is the largest component of lignocellulosic biomass (Yu et al., 2017). Cellulose fibrils are aggregated while reinforcing the crystalline matrix structure through the existence of numerous intramolecular or intermolecular hydrogen bonds (Haldar & Purkait, 2020). The robust and intricate network of hydrogen bonds between hydroxyl groups of cellulose chains serves to stabilize and organize the cellulose molecules into a well-structured arrangement through crystalline packing, resulting in the formation of elongated and infinite crystalline rods along the microfibrils axis (Rajinipriya et al., 2018). Consequently, cellulose necessitates elevated pressure and temperature to dismantle its large crystalline structure for potential utilization (Haldar et al., 2018). Cellulose has been utilized in various applications over the past few decades and remains highly promising when appropriately treated or modified, owing to its physicochemical characteristics, biodegradability, biocompatibility, and renewability (Liao et al., 2020).

Hemicellulose is another form of polysaccharide composed of multiple carbohydrate monomers, mainly xylose, arabinose, mannose, and glucose in varying ratios in different biomass samples (Negahdar et al., 2016; Yu et al., 2017). The hemicellulose structure may contain sugar acids such as methylgalacturonic, galacturonic, and glucuronic acids, and acetyl groups (Liao et al., 2020; Zheng et al., 2014). Hemicellulose can be easily transformed due to its highly branched and amorphous structure (Luo et al., 2019). It also exhibits a significantly reduced degree of polymerization, ranging from 50 – 200 U, which is notably lower compared to cellulose (Luo et al., 2019; Yu et al., 2017). Other than that, hemicellulose has more instability compared to cellulose, thereby making it susceptible to degradation under heat treatment conditions. Hemicellulose possesses exceptional characteristics,

including biodegradability, biocompatibility, and bioactivity, making it suitable for a wide range of applications such as food, medicine, energy, chemical industry, and polymeric materials (Bian et al., 2013; Kapu & Trajano, 2014; Otieno & Ahring, 2012).

2.5 Oil palm (*Elaeis guineensis*)

Malaysia is globally acknowledged as the second largest producer of oil palm after Indonesia (Goggin & Murphy, 2018). The production of crude palm oil in Malaysia reached 14.5 million tons in 2023 (MPOB, 2023b). Therefore, the increasing of crude oil production will consequently increase the amount of oil palm waste as time goes on. The yearly output of solid biomass wastes, including oil palm trunks (OPT), palm kernel shells (PKS), mesocarp fiber (MF), empty fruit bunches (EFB), and oil palm fronds (OPF), exceeds 80 million tons/year (dry weight basis) (Megashah et al., 2018; Yiin et al., 2018). It is projected that these figures would rise by 40% by the year 2030 (Rupani et al., 2019). These wastes were intentionally left to decompose for mulching and recycling. Nevertheless, this process takes a significant amount of time, which could potentially lead to a severe ecological catastrophe (Awalludin et al., 2015).

OPF is one of the most abundant lignocellulosic biomass wastes which reached 47% out of the total oil palm industry (Nordin et al., 2017; Ong et al., 2021). According to previous research, OPF has the largest amount of lignin, nearly 31% followed by cellulose content ranging from 31 – 45.20% and hemicellulose content ranging from 17.10 – 19.20% (Kabir et al., 2017; Shah et al., 2017; Solikhah et al., 2018). Researchers are interested in using OPF to extract the main components of

lignocellulosic biomass for potential applications in producing activated carbon, corrosion inhibitors, biofuel production, and bioethanol production (Derman et al., 2018; Rashidi & Yusup, 2017; Shah et al., 2017; Sukiran et al., 2017). These applications aim to mitigate the negative environmental effects of global warming by utilizing natural waste products (Mahlia et al., 2019).

2.6 Lignin

Lignin is a complex, amorphous aromatic polymer that comprises a significant proportion of the cellular walls of vascular plants. It is the second most prevalent biopolymer, surpassed only by cellulose (Kai et al., 2016). Lignin, a prominent constituent of lignocellulosic biomass, comprises three elemental components, carbon, hydrogen, and oxygen (Fodil Cherif et al., 2020; Liao et al., 2020). The phenylpropanoid units of three aromatic alcohols, which are p-hydroxyphenyl (H) units, syringyl (S) units, and guaiacyl (G) units are connected by a variety of ether and carbon-carbon linkages as illustrated in Figure 2.4 (Katahira et al., 2018; Mei et al., 2019; Nasrun et al., 2023). The composition and amount of lignin vary depending on the source of biomass. Softwood plants consist mainly of G units and typically contain a high amount of lignin, reaching up to 30%. In contrast, hardwood plants contain lignin from both G and S units and often have a moderate lignin content, of up to 25% (Suota et al., 2021; Takada et al., 2020; Vaidya et al., 2022).

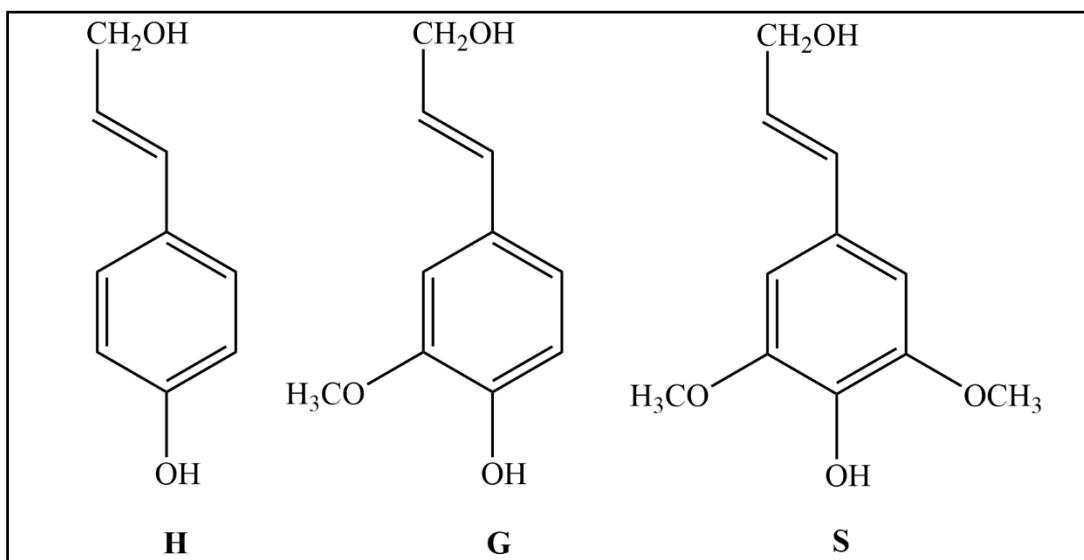


Figure 2.4: Main phenylpropanoid units of lignin (Katahira et al., 2018; Mei et al., 2019; Nasrun et al., 2023).

Each of these hydroxycinnamic alcohols is made up of an aromatic moiety and a side chain consisting of three carbons, which are identified as α , β , and γ (Laurichesse & Avérous, 2014; Liao et al., 2020; Tribot et al., 2019). Several linkages such as alkyl-aryl ether (β -O-4), phenylcoumaran (β -5), 1,2-diaryl-propane (β -1), diaryl (5-5), diaryl ether (4-O-5), and resinol (β - β) as represented in Figure 2.5, has been discovered in lignin units in varying quantities (Katahira et al., 2018; Mei et al., 2019; Schutyser et al., 2018). The cleavable linkages, particularly α -O-4 and β -O-4 are the primary bonds in lignin structures (Evstigneyev & Shevchenko, 2019). It is commonly recognized that when C- β is in its most reactive state, β -O-4, β -5, and β - β are produced in large quantities. Approximately 50% of lignin connections consist of the major inter-lignin bonds, β -O-4. In conjunction with the α -O-4 linkages, the ether bonds have been identified as the least resistant and most susceptible to cleavage in comparison to other bonds (Tribot et al., 2019). Previous research indicated that hardwood plants predominantly have β -O-4 lignin linkages, meanwhile, softwood plants had a higher proportion of β -5 and 5-5 lignin linkages (Mei et al., 2019).

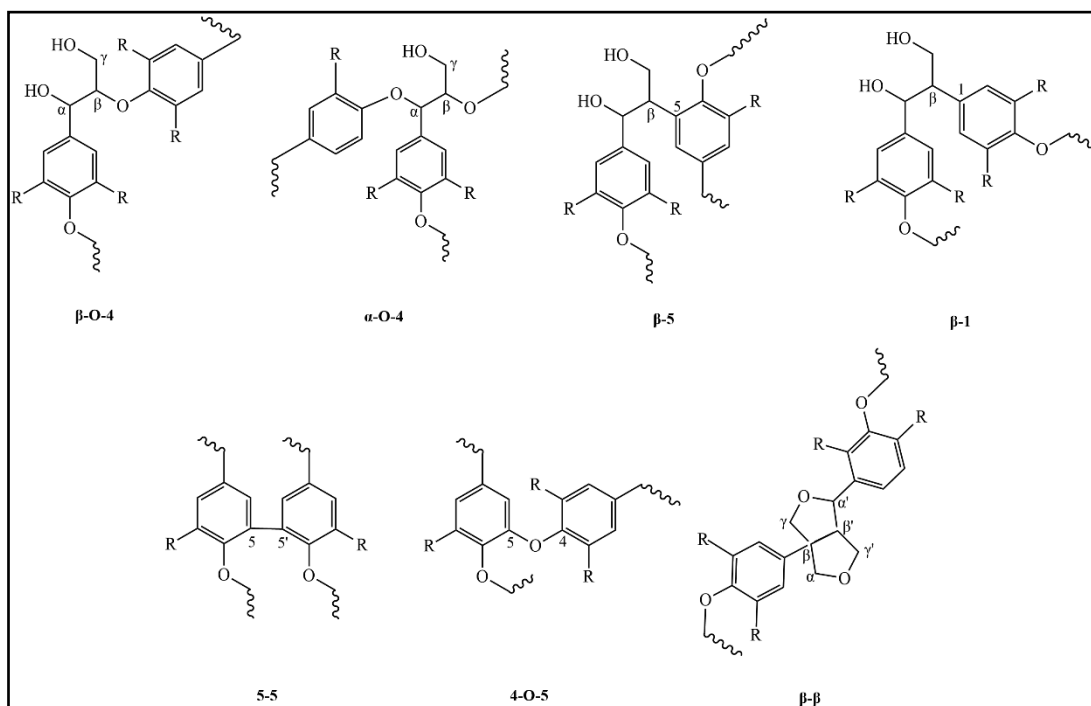


Figure 2.5: Several linkages in the lignin structures (Katahira et al., 2018; Mei et al., 2019; Schutyser et al., 2018).

The several advantageous properties of lignin, including its high carbon content, thermal stability, biodegradability, antioxidant activity, and good stiffness, have generated significant interest in the development of value-added products for diverse applications utilizing this natural polyphenol (Hu et al., 2018; Kai et al., 2016). Previous studies have demonstrated the diverse applications of lignin, including its utilization as bioplastics (Brodin et al., 2017; Nair et al., 2018), dispersants (Huang et al., 2018; Qin et al., 2016), polyurethane foam (Luo et al., 2018), nanocomposites (Jiang et al., 2020; Zhang et al., 2020), biosurfactants (Fatriasari et al., 2020; Karimah et al., 2023), adsorbents (Alassod et al., 2020; Chen et al., 2020), fire-retardants (Liang et al., 2021), phenolic resins (Yang et al., 2021), wood adhesives (Gan et al., 2019), corrosion inhibitors (El-Deeb et al., 2018; Gao et al., 2021), and rust conversion studies (Nasrun et al., 2023).

2.7 Delignification process

Delignification is a procedure that aims to separate the primary constituents, namely lignin, cellulose, and hemicelluloses, from the lignocellulosic biomass. Lignin can be derived from various delignification processes, including Kraft pulping, soda pulping, and organosolv pulping (Ekielski & Mishra, 2020; Latif et al., 2022; Tribot et al., 2019). Prior research has indicated that various delignification methods have a significant impact on the extraction yields, lignin functionality, molar mass, and physicochemical properties. This is because several important factors, such as pH, temperature, pressure, and chemical load, can influence the extraction process (Liao et al., 2020; Schieppati et al., 2023). During the delignification process, the breaking of the ether and ester bonds in the larger lignin structure will be interrupted, causing the resultant fragments to dissolve and generate black liquor. Following the pulping procedure, the lignin can be extracted by precipitating the black liquor (Alves-Ferreira et al., 2021; Schieppati et al., 2023).

2.7.1 Organosolv pulping

Organosolv pulping which is also known as organic solvent-based pulping involves the use of organic solvents, such as organic acids and alcohols, to dissolve a significant portion of the lignin and extract fibers from the composite material, resulting in the production of pulp. The most common organic solvents used to extract lignin and hemicellulose from wood materials are ethanol, methanol, formic acid, acetic acid, or a mixture of water/organic solvents usually applied at high temperatures ranging from 100 – 250 °C (Alves-Ferreira et al., 2021; Figueiredo et al., 2018; Takada et al., 2020; Vaidya et al., 2022). It is possible to carry out the pulping process with or without the use of catalysts such as H₂SO₄, HCl, H₃PO₄, acetic acid, formic acid, or